

X-ray Thomson scattering absolute intensity from the f-sum rule in the imaginary-time domain

Tobias Dornheim,^{1, 2, *} Tilo Döppner,³ Andrew D. Baczewski,⁴ Panagiotis Tolias,⁵ Maximilian P. Böhme,^{1, 2, 6} Zhandos A. Moldabekov,^{1, 2} Divyanshu Ranjan,^{7, 2} David A. Chapman,⁸ Michael J. MacDonald,³ Thomas R. Preston,⁹ Dominik Kraus,^{7, 2} and Jan Vorberger²

¹Center for Advanced Systems Understanding (CASUS), D-02826 Görlitz, Germany

²Helmholtz-Zentrum Dresden-Rossendorf (HZDR), D-01328 Dresden, Germany

³Lawrence Livermore National Laboratory (LLNL), California 94550 Livermore, USA

⁴Center for Computing Research, Sandia National Laboratories, Albuquerque NM 87185 USA

⁵Space and Plasma Physics, Royal Institute of Technology (KTH), Stockholm, SE-100 44, Sweden

⁶Technische Universität Dresden, D-01062 Dresden, Germany

⁷Institut für Physik, Universität Rostock, D-18057 Rostock, Germany

⁸First Light Fusion, Yarnton, Oxfordshire, United Kingdom

⁹European XFEL, D-22869 Schenefeld, Germany

We evaluate the f-sum rule on the dynamic structure factor in the imaginary-time domain as a formally exact and simulation-free means of normalizing X-Ray Thomson Scattering (XRTS) spectra. This circumvents error-prone real-time deconvolution of the source function and facilitates calculating the static structure factor from the properly normalized imaginary-time correlation function. We apply our technique to two distinct sets of experimental data, finding that it is effective for both narrow and broad x-ray sources. This approach could be readily adapted to other scattering spectroscopies.

Introduction.— Matter at extreme temperatures ($T \sim 10^3 - 10^8$ K) and pressures ($P \sim 1 - 10^4$ Mbar) is ubiquitous throughout nature [1, 2] and occurs within astrophysical objects such as giant planet interiors [3] and brown dwarfs [4]. In addition, such high energy density (HED) conditions can be realized in the laboratory using different techniques [5]. Prominent examples include inertial confinement fusion [6] as it is realized at the National Ignition Facility (NIF) [7], and isochoric heating using free-electron X-ray laser beams [8]. Indeed, there have been a number of spectacular experimental achievements over the last years, including the observation of diamond formation at planetary interior conditions by Kraus *et al.* [9, 10] and a number of breakthroughs related to nuclear fusion at NIF [11, 12].

However, the extreme conditions render the diagnostics a formidable challenge as often even basic parameters such as the temperature cannot be directly measured. Instead, they have to be inferred indirectly from other observations. In this regard, the X-ray Thomson scattering (XRTS) technique [13, 14] has emerged as a widely used tool that is available both in the HED regime [8, 15, 16] and at ambient conditions [17]. The measured XRTS intensity $I(\mathbf{q}, \omega)$ (with \mathbf{q} and ω being the scattering momentum and energy, respectively) can be expressed as [18]

$$I(\mathbf{q}, \omega) = A S_{ee}(\mathbf{q}, \omega) \circledast R(\omega), \quad (1)$$

with $S_{ee}(\mathbf{q}, \omega)$ being the electron-electron dynamic structure factor and $R(\omega)$ being the combined source and instrument function (SIF). The latter is often known from

either separate source monitoring or the characterization of backlighter sources [19]. Moreover, A denotes a normalization constant that is *a priori* unknown.

In practice, the numerical deconvolution of Eq. (1) to extract $S_{ee}(\mathbf{q}, \omega)$ is unstable due to the inevitable noise in the experimental data. Therefore, the traditional way to interpret an XRTS signal is to construct a model $S_{\text{model}}(\mathbf{q}, \omega)$ and then convolve it with $R(\omega)$. Comparing with the experimental signal then allows one to obtain the unknown variables such as the temperature, which are being treated as free parameters [20]. On the one hand, this *forward modeling* procedure gives one access e.g. to the equation-of-state [21, 22], which is of prime importance for a gamut of practical applications. On the other hand, the inferred system parameters can strongly depend on the employed model assumptions, such as the Chihara decomposition into *bound* and *free* electrons [23, 24].

Very recently, Dornheim *et al.* [18, 25, 26] have suggested to instead analyze the two-sided Laplace transform of $S_{ee}(\mathbf{q}, \omega)$,

$$F_{ee}(\mathbf{q}, \tau) = \mathcal{L}[S_{ee}(\mathbf{q}, \omega)] = \int_{-\infty}^{\infty} d\omega e^{-\hbar\omega\tau} S_{ee}(\mathbf{q}, \omega), \quad (2)$$

which has a number of key advantages. First, the deconvolution with respect to the SIF is straightforward in the Laplace domain, see Eq. (3) below. Second, the Laplace transform is remarkably robust with respect to noise in the intensity, see Ref. [18] and the Supplemental Material [27]. Third, Eq. (2) directly corresponds to the imaginary-time correlation function (ITCF) $F_{ee}(\mathbf{q}, \tau)$. The latter corresponds to the usual intermediate scattering function $F_{ee}(\mathbf{q}, t)$, but evaluated at an imaginary argument $t = -i\hbar\tau$, with $\tau \in [0, \beta]$ and $\beta = 1/k_B T$ being

* t.dornheim@hzdr.de

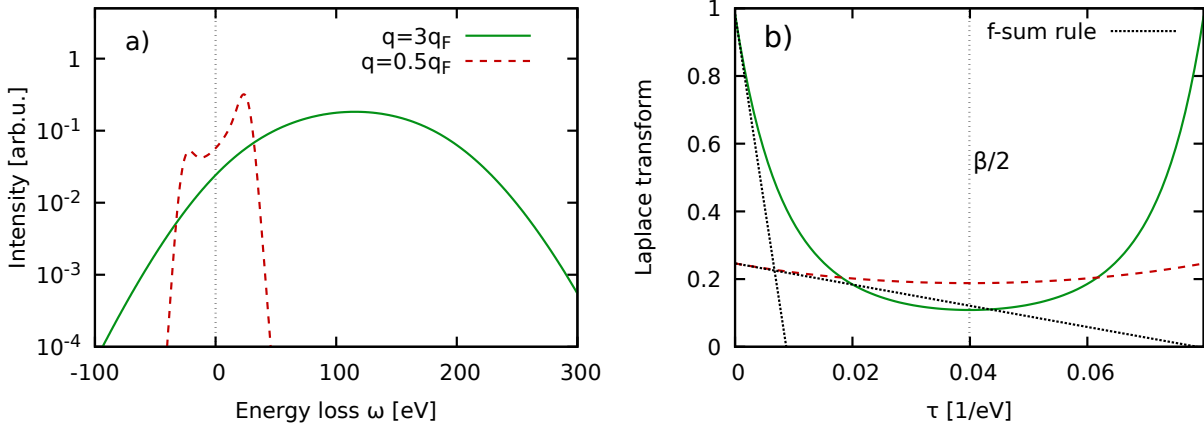


FIG. 1. a) Synthetic XRTS intensity for a uniform (free) electron gas at $r_s = 2$ and $\Theta = 1$ ($T = 12.53$ eV) with the Fermi wave number $q_F = 1.81 \text{ \AA}^{-1}$. The dynamic structure factors $S_{ee}(\mathbf{q}, \omega)$ for $q = 3q_F$ (solid green) and $q = 0.5q_F$ (dashed red) have been convolved with a Gaussian instrument function of width $\sigma = 3.33$ eV. b) Corresponding ITCF, cf. Eq. (2). The dotted black lines show asymptotic linear expansions around $\tau = 0$ and have been obtained from the f-sum rule.

the usual inverse temperature. In thermodynamic equilibrium, $F_{ee}(\mathbf{q}, \tau)$ is symmetric around $\tau = \beta/2$, which means that Eq. (2) allows one to extract the temperature without any models or approximations. In addition, knowledge of the properly normalized ITCF is related to the electron-electron static structure factor via $S_{ee}(\mathbf{q}) = F_{ee}(\mathbf{q}, 0)$.

We stress that, due to the uniqueness of the two-sided Laplace transform, the ITCF contains exactly the same information as $S_{ee}(\mathbf{q}, \omega)$, albeit in an unfamiliar representation. This theme has been explored in the recent Refs. [26, 28–30], where it has been argued that the imaginary-time domain can give direct access to many properties, including quasi-particle energies and the static limit of the linear density response function. The latter points the way toward experimental measurements of the exchange-correlation kernel of real materials, which will be of high value for the benchmarking and further development of *ab initio* density functional theory (DFT) simulations [31–33]. Yet, these promising possibilities require accurate and absolute knowledge of $F_{ee}(\mathbf{q}, \tau)$ itself, which, in turn, makes it necessary to determine the generally unknown normalization constant A , cf. Eq. (1).

In this Letter, we demonstrate how to determine the normalization of an XRTS signal by utilizing the well-known f-sum rule in the imaginary-time domain. Our method works for all wave numbers covering both the collective and the single-particle regime. We apply it to measurements at HED conditions taken at NIF [34] and ambient conditions investigated at the European XFEL [35]. Finally, the general validity of the f-sum rule makes it available even in the most general case of nonequilibrium [36].

Methods.— A key advantage of the two-sided Laplace transform defined in Eq. (2) above is the convolution the-

orem

$$AF_{ee}(\mathbf{q}, \tau) = A\mathcal{L}[S_{ee}(\mathbf{q}, \omega)] = \frac{\mathcal{L}[I(\mathbf{q}, \omega)]}{\mathcal{L}[R(\omega)]}, \quad (3)$$

which gives us straightforward access to $AF_{ee}(\mathbf{q}, \tau)$.

To determine the normalization constant A , we consider the frequency moments of the dynamic structure factor [29]

$$M_\alpha^S = \int_{-\infty}^{\infty} d\omega S_{ee}(\mathbf{q}, \omega) \omega^\alpha. \quad (4)$$

It is easy to see that all positive integer M_α^S can be obtained from τ -derivatives of the ITCF around $\tau = 0$ [26, 30],

$$M_\alpha^S = \frac{(-1)^\alpha}{\hbar^\alpha} \left. \frac{\partial^\alpha}{\partial \tau^\alpha} F_{ee}(\mathbf{q}, \tau) \right|_{\tau=0}. \quad (5)$$

The final ingredient to our approach is given by the f-sum rule [37] $M_1^S = \hbar q^2/2m_e$, which, when being combined with Eqs. (1), (3) and (5), leads to the relation

$$A = -\frac{2m_e}{(\hbar q)^2} \left. \frac{\partial}{\partial \tau} \frac{\mathcal{L}[I(\mathbf{q}, \omega)]}{\mathcal{L}[R(\omega)]} \right|_{\tau=0}. \quad (6)$$

Eq. (6) implies that we can directly calculate A from the slope of the ratio of the Laplace transforms of the intensity and the SIF around the origin.

Results.— To illustrate the physical origin of our idea, we show synthetic intensities based on a uniform electron gas (UEG) model [38–41] at a metallic density with the Wigner-Seitz radius [42] $r_s = 2$ and $T = 12.53$ eV (i.e., at the electronic Fermi temperature [42] $\Theta = k_B T/E_F = 1$) for different scattering momenta in Fig. 1a). The solid green curve has been obtained for $|\mathbf{q}| = 3q_F$, q_F being the Fermi wave number, corresponding to a backscattering

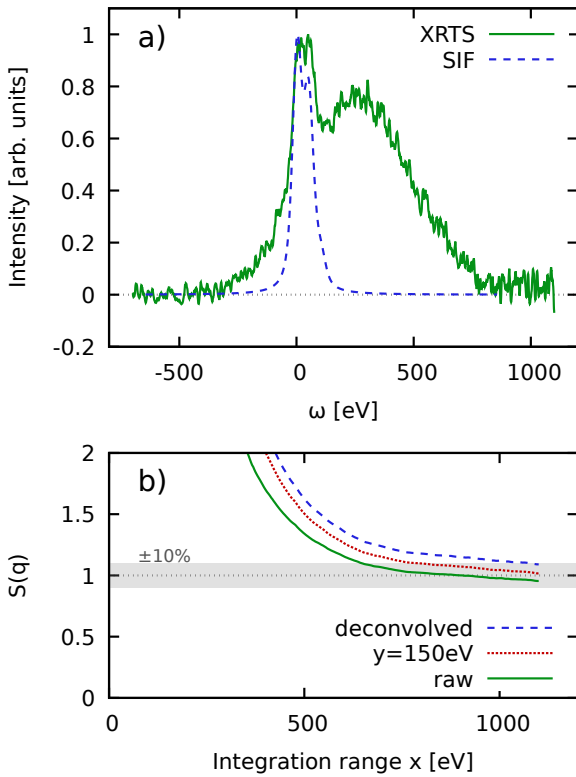


FIG. 2. a) XRTS intensity (solid green) and model SIF (dashed blue) for a NIF shot of strongly compressed Be [34] with a nominal temperature and density of $T = 119 \pm 10/50$ eV and $n = 1.9 \pm 0.2 \times 10^{24}$ cm $^{-3}$. The scattering angle is given by $\theta = 120^\circ$, corresponding to $q = 7.89$ Å $^{-1}$. b) Convergence of the normalized static structure factor $S_{ee}(\mathbf{q}) = F_{ee}(\mathbf{q}, 0)$ as a function of the symmetrically truncated integration range x [27]. Dashed blue: full evaluation of Eq. (6); solid green: setting $\mathcal{L}[R(\omega)] \equiv 1$; dotted red: truncating the wings of the model SIF at $y = \pm 150$ eV.

geometry. In this noncollective single-particle regime, the intensity is given by a single broad peak encompassing both positive and negative frequencies. The dashed red curve has been computed for $|\mathbf{q}| = 0.5q_F$, thereby probing the collective plasmon excitation around the plasma frequency ω_p . In Fig. 1b), we show the corresponding results for the ITCF $F_{ee}(\mathbf{q}, \tau)$, cf. Eq. (2). Both curves are symmetric around the same value of $\tau = \beta/2$, which has been used in Refs. [18, 25] as a method of temperature diagnostics. In the present work, we focus on the vicinity of $\tau = 0$, where the ITCF is asymptotically described by the f-sum rule. The corresponding linear expansions (see also Ref. [30]) around $\tau = 0$ are depicted as the dotted black lines, and asymptotically agree with the UEG data for both values of q . Relating the numerical derivative of the (unnormalized) two-sided Laplace transform of the XRTS signal $I(\mathbf{q}, \omega)$ to the slope of the true ITCF that is known from the f-sum rule via Eq. (6) thus provides a straightforward pathway to determine the normalization A .

In Fig. 2a), we show an XRTS signal (solid green) that has been obtained for warm dense beryllium at the NIF by Döppner *et al.* [34]. Capsules with an outer layer of beryllium and a core of air were compressed using 184 laser beams of the NIF and an additional 8 laser beams where used as backscatterers to generate the x-rays for the scattering diagnostics. The created conditions at $t = 0.48$ ns after peak x-ray emission were diagnosed to be at a temperature of $T = 119 \pm 10/50$ eV and a density of $n = 1.9 \pm 0.2 \times 10^{24}$ cm $^{-3}$ corresponding to five-fold compression of solid beryllium [34]. A practical obstacle regarding the evaluation of Eq. (6) is given by the limited frequency range of the detector. In practice, we symmetrically truncate the integration range for the two-sided Laplace transform of $I(\mathbf{q}, \omega)$ [Eq. (2)] at $\pm x$. In Fig. 2b), we show the convergence of the thus determined, properly normalized static structure factor $S_{ee}(\mathbf{q}) = F_{ee}(\mathbf{q}, 0)$ with x . The solid green curve has been computed without taking into account the impact of $R(\omega)$ [i.e., setting $\mathcal{L}[R(\omega)] \equiv 1$ in Eq. (6)], whereas the dashed blue curve is based on the full evaluation of Eq. (6). Both curves exhibit the same qualitative behavior and converge around $S_{ee}(\mathbf{q}) = 1$ in the limit of large x . This is indeed the expected value for $S_{ee}(\mathbf{q})$ of Be in the single-particle limit of large q at these conditions, which nicely confirms our approach. Finally, the dotted red curve has been obtained by truncating the SIF around $y = \pm 150$ eV. This is motivated by the unclear shape of the wings of the depicted model for $R(\omega)$, which only slowly decay for large ω . We find that the truncation leads to a normalization that is located between the green and blue results. This clearly illustrates the practical impact of the SIF onto the interpretation of XRTS experiments, and highlights the need for improved source function characterization [19] for future experiments.

To demonstrate the versatility of our idea, we next consider an XRTS measurement of diamond at ambient conditions that has been performed at the European XFEL by Voigt *et al.* [35] in Fig. 3. The wave number is given by $q = 5.94$ Å $^{-1}$, which is close to, though not directly on top of, a Bragg peak. This makes the correct value of $S_{ee}(\mathbf{q})$ unclear prior to our analysis. We note the high accuracy of the measured intensity (solid green) over four orders of magnitude, and the remarkably narrow width of the SIF (dashed blue). In addition, Voigt *et al.* [35] have captured the entire relevant down-shifted (i.e., $\omega > 0$) spectral range well beyond the K-shell feature around $\omega = 290$ eV. This is essential for the proper estimation of the normalization as we shall elaborate in more detail in the discussion below. In Fig. 3b), we show the corresponding convergence of $S_{ee}(\mathbf{q})$ with x . Evidently, we cannot resolve any significant impact of the SIF, which is unsurprising given its narrow bandwidth. We observe a monotonic behavior for $x \gtrsim 400$ eV that is well reproduced by a simple quadratic fit (dotted yellow). To get an empirical estimate for the associated uncertainty, we also perform quadratic fits for $x \gtrsim 300$ eV and $x \gtrsim 500$ eV, which are depicted as the light grey area. This leads

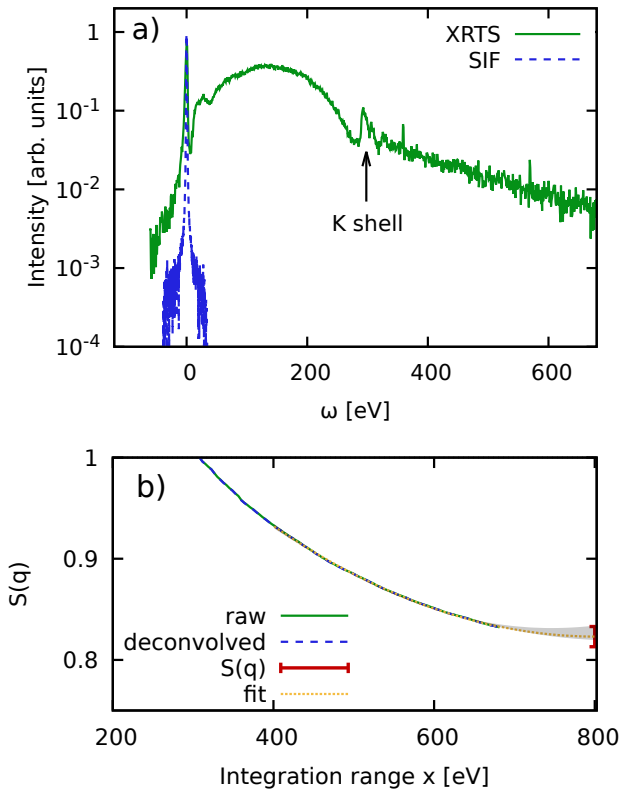


FIG. 3. a) XRTS intensity (solid green) and SIF (dashed blue) of carbon measured by Voigt *et al.* [35] at the European XFEL. The scattering angle and wave number are given by $\theta = 155^\circ$ and $q = 5.94 \text{ \AA}^{-1}$. b) Corresponding convergence of the normalized static structure factor $S_{ee}(\mathbf{q}) = F_{ee}(\mathbf{q}, 0)$ with the integration range x [27]. The dotted yellow curve shows an empirical quadratic fit to the deconvolved data for $x \in [400, 680] \text{ eV}$, and the red data point marks our final estimation of $S_{ee}(\mathbf{q}) = 0.823 \pm 0.01$.

to our final estimate for the static structure factor as $S_{ee}(\mathbf{q}) = 0.823 \pm 0.01$. An additional analysis of the spectrally resolved contributions to Eq. (6) is given in the Supplemental Material [27].

Discussion.— We have presented a new, simulation-free approach for the computation of the a-priori unknown normalization of XRTS measurements. Our approach works for any degree of collectivity, and over a broad range of temperatures including ambient conditions and the HED regime. Moreover, it is not restricted to thermal equilibrium and, therefore, can readily be applied e.g. to self-scattering experiments that cannot be described rigorously with existing simulation capabilities. The high stability of our method with respect to the inevitable noise in the experimental data, and the convergence with respect to the integration boundaries are analyzed in more detail in the Supplemental Material [27].

We are convinced that our scheme will open up a great variety of possibilities for interesting future work. A

starting point can be the rigorous quantification of the remaining uncertainty in the normalization due to effects such as q -vector blurring or the potential small dependence of q on the scattering frequency ω [18]. An additional issue emerges for XRTS measurements of heavier elements, where the excitation of tightly bound-core electrons to the continuum will lead to contributions in $S_{ee}(\mathbf{q}, \omega)$ and, thus, $I(\mathbf{q}, \omega)$ that are outside of the available detector range. On the one hand, an incomplete spectral range prevents the direct determination of the normalization in either the ω - or τ -representation by default. On the other hand, XRTS is an inelastic spectroscopy and the scattering intensity contributed by processes involving core electrons will decay rapidly with increasing binding energy unless the probe beam energy is nearly resonant with a real transition [43]. One can imagine quantifying the uncertainty that the finite detection bandwidth introduces by predicting the weight of low-intensity high-energy features associated with bound-free [44] and bound-bound [45] transitions involving deeply bound core electrons with highly efficient all-electron average atom methods [46].

From a physical perspective, the normalization gives us direct access to the static structure factor $S_{ee}(\mathbf{q})$, which is important in its own right. This additional bit of information might help to further constrain the forward modelling of XRTS measurements via chemical models [8, 14, 24] or *ab initio* simulations [47–50]. In addition, it makes XRTS a useful tool for the probing of electron–electron correlations on different length scales. The fact that XRTS measurements allow us to check the integration over the available spectral range can also be useful as a rigorous benchmark for X-ray diffraction [51].

We again note that the ITCF $F_{ee}(\mathbf{q}, \tau)$, by definition, contains the same information as the dynamic structure factor $S_{ee}(\mathbf{q}, \omega)$. Experimental results for the properly normalized ITCF will, therefore, allow us to extract a wealth of additional information from XRTS measurements beyond the temperature [18, 25], including quasi-particle excitation energies and even nontrivial processes such as the roton-type feature that has recently been reported in an interacting electron gas at low density [26, 28, 52]. In this context, a particularly important relation is given by the imaginary-time version of the fluctuation–dissipation theorem [26],

$$\chi(\mathbf{q}, 0) = -n \int_0^\beta d\tau F_{ee}(\mathbf{q}, \tau) , \quad (7)$$

that connects the ITCF with the static limit of the linear density response function, $\chi(\mathbf{q}, 0)$. In particular, Eq. (7) gives one direct access to the static exchange–correlation kernel $K_{xc}(\mathbf{q})$, which is a key property in quantum many-body theory [29, 31]. In this way, our idea will open up the possibility to rigorously test existing kernels against XRTS measurements at modern XFEL facilities such as the European XFEL [53].

ACKNOWLEDGMENTS

This work was partially supported by the Center for Advanced Systems Understanding (CASUS) which is financed by Germany's Federal Ministry of Education and Research (BMBF) and by the Saxon state government out of the State budget approved by the Saxon State Parliament. This work has received funding from the European Research Council (ERC) under the European Union's Horizon 2022 research and innovation programme (Grant agreement No. 101076233, "PREXTREME"). The work of Ti. D. and M. J. M. was performed under the auspices of the U.S. Department of Energy by Lawrence Livermore National Laboratory

under Contract No. DE-AC52-07NA27344. A.D.B. acknowledges support from Sandia's Laboratory Directed Research and Development Program and US Department of Energy Science Campaign 1. Sandia National Laboratories is a multimission laboratory managed and operated by National Technology and Engineering Solutions of Sandia, LLC, a wholly-owned subsidiary of Honeywell International Inc., for the U.S. Department of Energy's National Nuclear Security Administration under contract DE-NA0003525. The PIMC calculations for the synthetic UEG data were carried out at the Norddeutscher Verbund für Hoch- und Höchstleistungsrechnen (HLRN) under grant shp00026, and on a Bull Cluster at the Center for Information Services and High Performance Computing (ZIH) at Technische Universität Dresden.

[1] R.P. Drake, *High-Energy-Density Physics: Foundation of Inertial Fusion and Experimental Astrophysics*, Graduate Texts in Physics (Springer International Publishing, 2018).

[2] V. E. Fortov, "Extreme states of matter on earth and in space," *Phys.-Usp* **52**, 615–647 (2009).

[3] Alessandra Benuzzi-Mounaix, Stéphane Mazevet, Alessandra Ravasio, Tommaso Vinci, Adrien De-noeud, Michel Koenig, Nourou Amadou, Erik Brambrink, Floriane Festa, Anna Levy, Marion Harmand, Stéphanie Brygoo, Gael Huser, Vanina Recoules, Johan Bouchet, Guillaume Morard, François Guyot, Thibaut de Ressegueir, Kohei Myanishi, Norimasa Ozaki, Fabien Dorchies, Jérôme Gaudin, Pierre Marie Leguay, Olivier Peyrusse, Olivier Henry, Didier Raffestin, Sébastien Le Pape, Ray Smith, and Riccardo Musella, "Progress in warm dense matter study with applications to planetology," *Phys. Scripta* **T161**, 014060 (2014).

[4] A. Becker, W. Lorenzen, J. J. Fortney, N. Nettelmann, M. Schöttler, and R. Redmer, "Ab initio equations of state for hydrogen (h-reos.3) and helium (he-reos.3) and their implications for the interior of brown dwarfs," *Astrophys. J. Suppl. Ser* **215**, 21 (2014).

[5] K. Falk, "Experimental methods for warm dense matter research," *High Power Laser Sci. Eng* **6**, e59 (2018).

[6] S. X. Hu, B. Militzer, V. N. Goncharov, and S. Skupsky, "First-principles equation-of-state table of deuterium for inertial confinement fusion applications," *Phys. Rev. B* **84**, 224109 (2011).

[7] E. I. Moses, R. N. Boyd, B. A. Remington, C. J. Keane, and R. Al-Ayat, "The national ignition facility: Ushering in a new age for high energy density science," *Physics of Plasmas* **16**, 041006 (2009).

[8] D. Kraus, B. Bachmann, B. Barbrel, R. W. Falcone, L. B. Fletcher, S. Frydrych, E. J. Gamboa, M. Gauthier, D. O. Gericke, S. H. Glenzer, S. Göde, E. Granados, N. J. Hartley, J. Helfrich, H. J. Lee, B. Nagler, A. Ravasio, W. Schumaker, J. Vorberger, and T. Döppner, "Characterizing the ionization potential depression in dense carbon plasmas with high-precision spectrally resolved x-ray scattering," *Plasma Phys. Control Fusion* **61**, 014015 (2019).

[9] D. Kraus, A. Ravasio, M. Gauthier, D. O. Gericke, J. Vorberger, S. Frydrych, J. Helfrich, L. B. Fletcher, G. Schau-
mann, B. Nagler, B. Barbrel, B. Bachmann, E. J. Gamboa, S. Göde, E. Granados, G. Gregori, H. J. Lee, P. Neu-
mayer, W. Schumaker, T. Döppner, R. W. Falcone, S. H. Glenzer, and M. Roth, "Nanosecond formation of dia-
mond and lonsdaleite by shock compression of graphite," *Nature Communications* **7**, 10970 (2016).

[10] D. Kraus, J. Vorberger, A. Pak, N. J. Hartley, L. B. Fletcher, S. Frydrych, E. Galtier, E. J. Gamboa, D. O. Gericke, S. H. Glenzer, E. Granados, M. J. MacDonald, A. J. MacKinnon, E. E. McBride, I. Nam, P. Neu-
mayer, M. Roth, A. M. Saunders, A. K. Schuster, P. Sun, T. van Driel, T. Döppner, and R. W. Falcone, "Formation of diamonds in laser-compressed hydrocarbons at planetary interior conditions," *Nature Astronomy* **1**, 606–611 (2017).

[11] H. Abu-Shawareb *et al.* (Indirect Drive ICF Collaboration), "Lawson criterion for ignition exceeded in an inertial fusion experiment," *Phys. Rev. Lett.* **129**, 075001 (2022).

[12] A. B. Zylstra, O. A. Hurricane, D. A. Callahan, A. L. Kritcher, J. E. Ralph, H. F. Robey, J. S. Ross, C. V. Young, K. L. Baker, D. T. Casey, T. Döppner, L. Di-
vol, M. Hohenberger, S. Le Pape, A. Pak, P. K. Patel, R. Tommasini, S. J. Ali, P. A. Amendt, L. J. Atherton, B. Bachmann, D. Bailey, L. R. Benedetti, L. Berzak Hop-
kins, R. Betti, S. D. Bhandarkar, J. Biener, R. M. Bionta, N. W. Birge, E. J. Bond, D. K. Bradley, T. Braun, T. M. Briggs, M. W. Bruhn, P. M. Celliers, B. Chang, T. Chapman, H. Chen, C. Choate, A. R. Christopherson, D. S. Clark, J. W. Crippen, E. L. Dewald, T. R. Dittrich, M. J. Edwards, W. A. Farmer, J. E. Field, D. Fittinghoff, J. Frenje, J. Gaffney, M. Gatu Johnson, S. H. Glenzer, G. P. Grim, S. Haan, K. D. Hahn, G. N. Hall, B. A. Hammel, J. Harte, E. Hartouni, J. E. Heebner, V. J. Hernandez, H. Herrmann, M. C. Herrmann, D. E. Hinkel, D. D. Ho, J. P. Holder, W. W. Hsing, H. Huang, K. D. Humbird, N. Izumi, L. C. Jarrott, J. Jeet, O. Jones, G. D. Kerbel, S. M. Kerr, S. F. Khan, J. Kilkenny, Y. Kim, H. Geppert Kleinrath, V. Geppert Kleinrath, C. Kong, J. M. Koning, J. J. Kroll, M. K. G. Kruse, B. Kus-
towski, O. L. Landen, S. Langer, D. Larson, N. C. Lemos, J. D. Lindl, T. Ma, M. J. MacDonald, B. J. MacGowan, A. J. Mackinnon, S. A. MacLaren, A. G. MacPhee,

M. M. Marinak, D. A. Mariscal, E. V. Marley, L. Masse, K. Meaney, N. B. Meezan, P. A. Michel, M. Millot, J. L. Milovich, J. D. Moody, A. S. Moore, J. W. Morton, T. Murphy, K. Newman, J.-M. G. Di Nicola, A. Nikroo, R. Nora, M. V. Patel, L. J. Pelz, J. L. Peterson, Y. Ping, B. B. Pollock, M. Ratledge, N. G. Rice, H. Rinderknecht, M. Rosen, M. S. Rubery, J. D. Salmonson, J. Sater, S. Schiaffino, D. J. Schlossberg, M. B. Schneider, C. R. Schroeder, H. A. Scott, S. M. Sepke, K. Sequoia, M. W. Sherlock, S. Shin, V. A. Smalyuk, B. K. Spears, P. T. Springer, M. Stadermann, S. Stoupin, D. J. Strozzi, L. J. Suter, C. A. Thomas, R. P. J. Town, E. R. Tubman, C. Trosseille, P. L. Volegov, C. R. Weber, K. Widmann, C. Wild, C. H. Wilde, B. M. Van Wonterghem, D. T. Woods, B. N. Woodworth, M. Yamaguchi, S. T. Yang, and G. B. Zimmerman, “Burning plasma achieved in inertial fusion,” *Nature* **601**, 542–548 (2022).

[13] J. Sheffield, D. Froula, S.H. Glenzer, and N.C. Luhmann, *Plasma Scattering of Electromagnetic Radiation: Theory and Measurement Techniques* (Elsevier Science, 2010).

[14] S. H. Glenzer and R. Redmer, “X-ray thomson scattering in high energy density plasmas,” *Rev. Mod. Phys* **81**, 1625 (2009).

[15] S. H. Glenzer, O. L. Landen, P. Neumayer, R. W. Lee, K. Widmann, S. W. Pollaine, R. J. Wallace, G. Gregori, A. Höll, T. Bornath, R. Thiele, V. Schwarz, W.-D. Kraeft, and R. Redmer, “Observations of plasmons in warm dense matter,” *Phys. Rev. Lett.* **98**, 065002 (2007).

[16] T. Döppner, O.L. Landen, H.J. Lee, P. Neumayer, S.P. Regan, and S.H. Glenzer, “Temperature measurement through detailed balance in x-ray thomson scattering,” *High Energy Density Physics* **5**, 182–186 (2009).

[17] R. Abela, A. Aghababyan, M. Altarelli, C. Altucci, G. Amatuni, P. Anfinrud, P. Audebert, V. Ayvazyan, N. Baboi, J. Baehr, V. Balandin, R. Bandelmann, J. Becker, B. Beutner, C. Blome, I. Bohnet, A. Bolzmann, C. Bostedt, Y. Bozhko, A. Brandt, S. Bratos, C. Bressler, O. Brovko, H. Brück, J. P. Carneiro, S. Casalbuoni, M. Castellano, P. Castro, L. Catani, A. Cavalleri, S. Celik, H. Chapman, D. Charalamidis, J. Chen, M. Chergui, S. Choroba, A. Cianchi, M. Clausen, E. Collet, H. Danared, C. David, W. Decking, M. Dehler, H. Delsim-Hashemi, G. Dipirro, B. Dobson, M. Dohlus, S. Duesterer, A. Eckhardt, H. J. Eckoldt, H. Edwards, B. Faatz, M. Fajardo, A. Fateev, J. Feldhaus, Y. Filipov, K. Floettmann, R. Follath, B. Fominykh, M. French, J. Frisch, L. Froehlich, E. Gadowinkel, L. García-Tabarés, J. J. Gareta, T. Garvey, F. Gel'mukhanov, U. Gensch, C. Gerth, M. Goerler, N. Golubeva, H. Graafsma, W. Graeff, O. Grimm, B. Grigoryan, G. Grübel, C. Gutt, K. Hacker, L. Haenisch, U. Hahn, J. Hajdu, J. H. Han, M. Hartrott, J. Havlicek, O. Hensler, K. Honkavaara, V. Honkimäki, T. Hott, M. R. Howells, M. Huening, H. Ihée, F. Ö. Ilday, R. Ischebeck, M. Jablonka, E. Jaeschke, K. Jensch, J. P. Jensen, S. Johnson, L. Juha, F. Kaerntner, R. Kammering, H. Kapitza, V. Katalev, B. Keil, S. Khodyachykh, R. Kienberger, J. W. Kim, Y. Kim, K. Klose, V. Kocharyan, W. Koehler, M. Koerfer, M. Kollewe, Q. Kong, W. Kook, D. Kostin, O. Kozlov, D. Kraemer, M. Krasilnikov, B. Krause, O. Krebs, J. Krzywinski, G. Kube, M. Kuhlmann, H. Laich, R. Lange, M. Larsson, R. W. Lee, A. Leuschner, H. Lierl, L. Lilje, T. Limberg, A. Lindenberg, D. Lipka, F. Loehl, K. Ludwig, M. Luong, C. Magne, A. Maquet, J. Marangos, C. Masciovecchio, M. Maslov, A. Matheisen, E. Matyushevskiy, O. Matzen, H. J. May, I. McNulty, D. McCormick, P. Meulen, N. Meyners, P. Michelato, N. Mildner, V. Miltchev, M. Minty, W. D. Moeller, T. Möller, L. Monaco, M. Nagl, O. Napoly, G. Neubauer, P. Nicolosi, A. Nienhaus, D. Noelle, T. Nunez, F. Obier, A. Oppelt, C. Pagan, R. Paparella, H. B. Pedersen, B. Petersen, B. Petrosyan, L. Petrosyan, A. Petrov, P. Piot, J. Pflueger, A. Plech, E. Ploenjes, L. Poletto, G. Pöplau, E. Prat, S. Prat, J. Prenting, D. Proch, D. Pugachov, H. Quack, B. Racky, D. Ramert, H. Redlin, K. Rehlich, R. Reining, H. Remde, D. Reschke, D. Richter, M. Richter, S. Riemann, D. Riley, I. Robinson, J. Roensch, F. Rosmej, M. Ross, J. Rossbach, V. Rybnikov, M. Sachwitz, E. Saldin, W. Sandner, J. Schäfer, T. Schilcher, H. Schlarb, M. Schloesser, V. Schlott, B. Schmidt, M. Schmitz, P. Schmueser, J. Schneider, E. Schneidmiller, F. Schotte, S. Schrader, S. Schreiber, C. Schroer, R. Schuch, H. Schulte-Schrepping, A. Schwarz, M. Seidel, J. Sekutowicz, P. Seller, D. Sellmann, F. Senf, D. Sertore, A. Shabunov, S. Simrock, W. Singer, H. Sinn, R. Smith, E. Sombrowski, A. A. Sorokin, E. Springate, M. Staack, L. Staykov, B. Steffen, B. Stephenson, F. Stephan, F. Stulle, E. Syresin, K. Sytchev, V. Sytchev, G. Tallents, S. Techert, N. Tesch, H. Thom, K. Tiedtke, M. Tischer, M. Tolan, S. Tolekis, F. Toral, R. Treusch, D. Trines, V. Tsakanov, I. Tsakov, T. Tschentscher, F. R. Ullrich, U. van Rienen, A. Variola, I. Vartaniants, E. Vogel, J. Vogel, R. Vuilleumier, H. Wabnitz, R. Wanzenberg, J. S. Wark, H. Weddig, T. Weiland, H. Weise, M. Wendt, R. Wenndorff, R. Wichmann, I. Will, A. Winter, K. Witte, K. Wittenburg, P. Wochner, T. Wohlenberg, J. Wojtkiewicz, A. Wolf, M. Wulff, M. Yurkov, I. Zagorodnov, P. Zambolin, K. Zapfe, P. Zeitoun, V. Ziemann, A. Zolotov, R. Brinkmann, H. J. Grabosch, and DESY, *XFEL: The European X-Ray Free-Electron Laser - Technical Design Report* (DESY, Hamburg, 2006) pp. 1–646.

[18] Tobias Dornheim, Maximilian P. Böhme, David A. Chapman, Dominik Kraus, Thomas R. Preston, Zhandos A. Moldabekov, Niclas Schlünzen, Attila Cangi, Tilo Döppner, and Jan Vorberger, “Imaginary-time correlation function thermometry: A new, high-accuracy and model-free temperature analysis technique for x-ray Thomson scattering data,” *Physics of Plasmas* **30**, 042707 (2023).

[19] M. J. MacDonald, A. M. Saunders, B. Bachmann, M. Bethkenhagen, L. Divol, M. D. Doyle, L. B. Fletcher, S. H. Glenzer, D. Kraus, O. L. Landen, H. J. LeFevre, S. R. Klein, P. Neumayer, R. Redmer, M. Schörner, N. Whiting, R. W. Falcone, and T. Döppner, “Demonstration of a laser-driven, narrow spectral bandwidth x-ray source for collective x-ray scattering experiments,” *Physics of Plasmas* **28**, 032708 (2021).

[20] M. F. Kasim, T. P. Galligan, J. Topp-Mugglestone, G. Gregori, and S. M. Vinko, “Inverse problem instabilities in large-scale modeling of matter in extreme conditions,” *Physics of Plasmas* **26** (2019), 10.1063/1.5125979, 112706.

[21] K. Falk, S.P. Regan, J. Vorberger, M.A. Barrios, T.R. Boehly, D.E. Fratanduono, S.H. Glenzer, D.G. Hicks, S.X. Hu, C.D. Murphy, P.B. Radha, S. Rothman, A.P. Jephcoat, J.S. Wark, D.O. Gericke, and G. Gregori,

“Self-consistent measurement of the equation of state of liquid deuterium,” *High Energy Density Physics* **8**, 76–80 (2012).

[22] K. Falk, E. J. Gamboa, G. Kagan, D. S. Montgomery, B. Srinivasan, P. Tzeferacos, and J. F. Benage, “Equation of state measurements of warm dense carbon using laser-driven shock and release technique,” *Phys. Rev. Lett.* **112**, 155003 (2014).

[23] J Chihara, “Difference in x-ray scattering between metallic and non-metallic liquids due to conduction electrons,” *Journal of Physics F: Metal Physics* **17**, 295–304 (1987).

[24] G. Gregori, S. H. Glenzer, W. Rozmus, R. W. Lee, and O. L. Landen, “Theoretical model of x-ray scattering as a dense matter probe,” *Phys. Rev. E* **67**, 026412 (2003).

[25] Tobias Dornheim, Maximilian Böhme, Dominik Kraus, Tilo Döppner, Thomas R. Preston, Zhando A. Moldabekov, and Jan Vorberger, “Accurate temperature diagnostics for matter under extreme conditions,” *Nature Communications* **13**, 7911 (2022).

[26] Tobias Dornheim, Zhando A. Moldabekov, Panagiotis Tolias, Maximilian Böhme, and Jan Vorberger, “Physical insights from imaginary-time density–density correlation functions,” (2022), 10.48550/ARXIV.2209.02254.

[27] See Supplemental Material for additional details.

[28] Tobias Dornheim, Jan Vorberger, Zhando A. Moldabekov, and Maximilian Böhme, “Analyzing x-ray thomson scattering experiments of warm dense matter in the imaginary-time domain: theoretical models and simulations,” (2022), 10.48550/ARXIV.2211.00579.

[29] Tobias Dornheim, Zhando A. Moldabekov, Kushal Ramakrishna, Panagiotis Tolias, Andrew D. Baczewski, Dominik Kraus, Thomas R. Preston, David A. Chapman, Maximilian P. Böhme, Tilo Döppner, Frank Graziani, Michael Bonitz, Attila Cangi, and Jan Vorberger, “Electronic density response of warm dense matter,” *Physics of Plasmas* **30**, 032705 (2023).

[30] Tobias Dornheim, Damar C. Wicaksono, Juan E. Suarez-Cardona, Panagiotis Tolias, Maximilian P. Böhme, Zhando A. Moldabekov, Michael Hecht, and Jan Vorberger, “Extraction of the frequency moments of spectral densities from imaginary-time correlation function data,” *Phys. Rev. B* **107**, 155148 (2023).

[31] Zhando A. Moldabekov, Maximilian Böhme, Jan Vorberger, David Blaschke, and Tobias Dornheim, “Ab Initio Static Exchange–Correlation Kernel across Jacob’s Ladder without Functional Derivatives,” *Journal of Chemical Theory and Computation* **19**, 1286–1299 (2023).

[32] Zhando A. Moldabekov, Mani Lokamani, Jan Vorberger, Attila Cangi, and Tobias Dornheim, “Non-empirical Mixing Coefficient for Hybrid XC Functionals from Analysis of the XC Kernel,” *The Journal of Physical Chemistry Letters* **14**, 1326–1333 (2023).

[33] Maximilian Schörner, Mandy Bethkenhagen, Tilo Döppner, Dominik Kraus, Siegfried H. Glenzer, and Ronald Redmer, “X-ray Thomson scattering spectra from DFT-MD simulations based on a modified Chihara formula,” (2023), 10.48550/ARXIV.2301.01545.

[34] T. Döppner, M. Bethkenhagen, D. Kraus, P. Neumayer, D. A. Chapman, B. Bachmann, R. A. Baggott, M. P. Böhme, L. Divol, R. W. Falcone, L. B. Fletcher, O. L. Landen, M. J. MacDonald, A. M. Saunders, M. Schörner, P. A. Sterne, J. Vorberger, B. B. L. Witte, A. Yi, R. Redmer, S. H. Glenzer, and D. O. Gericke, “Observing the onset of pressure-driven k-shell delocalization,” *Nature* (2023), 10.1038/s41586-023-05996-8.

[35] K. Voigt, M. Zhang, K. Ramakrishna, A. Amouretti, K. Appel, E. Brambrink, V. Cerantola, D. Chekrygina, T. Döppner, R. W. Falcone, K. Falk, L. B. Fletcher, D. O. Gericke, S. Göde, M. Harmand, N. J. Hartley, S. P. Hau-Riege, L. G. Huang, O. S. Humphries, M. Lokamani, M. Makita, A. Pelka, C. Prescher, A. K. Schuster, M. Šmid, T. Toncian, J. Vorberger, U. Zastrau, T. R. Preston, and D. Kraus, “Demonstration of an x-ray Raman spectroscopy setup to study warm dense carbon at the high energy density instrument of European XFEL,” *Physics of Plasmas* **28**, 082701 (2021).

[36] Jan Vorberger, Thomas R. Preston, Nikita Medvedev, Maximilian P. Böhme, Zhando A. Moldabekov, Dominik Kraus, and Tobias Dornheim, “Revealing non-equilibrium and relaxation in warm dense matter,” (2023), 10.48550/ARXIV.2302.11309.

[37] G. Giuliani and G. Vignale, *Quantum Theory of the Electron Liquid* (Cambridge University Press, Cambridge, 2008).

[38] T. Dornheim, S. Groth, and M. Bonitz, “The uniform electron gas at warm dense matter conditions,” *Phys. Reports* **744**, 1–86 (2018).

[39] T. Dornheim, S. Groth, J. Vorberger, and M. Bonitz, “Ab initio path integral Monte Carlo results for the dynamic structure factor of correlated electrons: From the electron liquid to warm dense matter,” *Phys. Rev. Lett.* **121**, 255001 (2018).

[40] Tobias Dornheim, Attila Cangi, Kushal Ramakrishna, Maximilian Böhme, Shigenori Tanaka, and Jan Vorberger, “Effective static approximation: A fast and reliable tool for warm-dense matter theory,” *Phys. Rev. Lett.* **125**, 235001 (2020).

[41] T. Dornheim, J. Vorberger, S. Groth, N. Hoffmann, Zh.A. Moldabekov, and M. Bonitz, “The static local field correction of the warm dense electron gas: An ab initio path integral Monte Carlo study and machine learning representation,” *J. Chem. Phys* **151**, 194104 (2019).

[42] Torben Ott, Hauke Thomsen, Jan Willem Abraham, Tobias Dornheim, and Michael Bonitz, “Recent progress in the theory and simulation of strongly correlated plasmas: phase transitions, transport, quantum, and magnetic field effects,” *The European Physical Journal D* **72**, 84 (2018).

[43] OS Humphries, RS Marjoribanks, QY Van Den Berg, EC Galtier, MF Kasim, HJ Lee, AJF Miscampbell, B Nagerl, R Royle, JS Wark, *et al.*, “Probing the electronic structure of warm dense nickel via resonant inelastic x-ray scattering,” *Physical Review Letters* **125**, 195001 (2020).

[44] AN Souza, DJ Perkins, CE Starrett, D Saumon, and SB Hansen, “Predictions of x-ray scattering spectra for warm dense matter,” *Physical Review E* **89**, 023108 (2014).

[45] Andrew D Baczewski, Thomas Hentschel, Alina Kononov, and Stephanie B Hansen, “Predictions of bound-bound transition signatures in x-ray Thomson scattering,” *arXiv preprint arXiv:2109.09576* (2021), 10.48550/arXiv.2109.09576.

[46] WR Johnson, J Nilsen, KT Cheng, *et al.*, “Thomson scattering in the average-atom approximation,” *Physical Review E* **86**, 036410 (2012).

[47] Maximilian Schörner, Bastian B. L. Witte, Andrew D.

Baczewski, Attila Cangi, and Ronald Redmer, “Ab initio study of shock-compressed copper,” *Phys. Rev. B* **106**, 054304 (2022).

[48] A. D. Baczewski, L. Shulenburger, M. P. Desjarlais, S. B. Hansen, and R. J. Magyar, “X-ray Thomson Scattering in Warm Dense Matter without the Chihara Decomposition,” *Phys. Rev. Lett* **116**, 115004 (2016).

[49] Kushal Ramakrishna, Attila Cangi, Tobias Dornheim, Andrew Baczewski, and Jan Vorberger, “First-principles modeling of plasmons in aluminum under ambient and extreme conditions,” *Phys. Rev. B* **103**, 125118 (2021).

[50] Zhando A. Moldabekov, Michele Pavanello, Maximilian P. Böhme, Jan Vorberger, and Tobias Dornheim, “Linear-response time-dependent density functional theory approach to warm dense matter with adiabatic exchange-correlation kernels,” *Phys. Rev. Res.* **5**, 023089 (2023).

[51] J. Vorberger and D. O. Gericke, “Ab initio approach to model x-ray diffraction in warm dense matter,” *Phys. Rev. E* **91**, 033112 (2015).

[52] Tobias Dornheim, Zhando Moldabekov, Jan Vorberger, Hanno Kähler, and Michael Bonitz, “Electronic pair alignment and roton feature in the warm dense electron gas,” *Communications Physics* **5**, 304 (2022).

[53] Thomas Tschentscher, Christian Bressler, Jan Grünert, Anders Madsen, Adrian P. Mancuso, Michael Meyer, Andreas Scherz, Harald Sinn, and Ulf Zastrau, “Photon Beam Transport and Scientific Instruments at the European XFEL,” *Applied Sciences* **7**, 592 (2017).

Supplemental Material: X-ray Thomson scattering absolute intensity from the f-sum rule in the imaginary-time domain

Tobias Dornheim,^{1, 2, *} Tilo Döppner,³ Andrew D. Baczewski,⁴ Panagiotis Tolias,⁵ Maximilian P. Böhme,^{1, 2, 6} Zhandos A. Moldabekov,^{1, 2} Divyanshu Ranjan,^{7, 2} David A. Chapman,⁸ Michael J. MacDonald,³ Thomas R. Preston,⁹ Dominik Kraus,^{7, 2} and Jan Vorberger²

¹Center for Advanced Systems Understanding (CASUS), D-02826 Görlitz, Germany

²Helmholtz-Zentrum Dresden-Rossendorf (HZDR), D-01328 Dresden, Germany

³Lawrence Livermore National Laboratory (LLNL), California 94550 Livermore, USA

⁴Center for Computing Research, Sandia National Laboratories, Albuquerque NM 87185 USA

⁵Space and Plasma Physics, Royal Institute of Technology (KTH), Stockholm, SE-100 44, Sweden

⁶Technische Universität Dresden, D-01062 Dresden, Germany

⁷Institut für Physik, Universität Rostock, D-18057 Rostock, Germany

⁸First Light Fusion, Yarnton, Oxfordshire, United Kingdom

⁹European XFEL, D-22869 Schenefeld, Germany

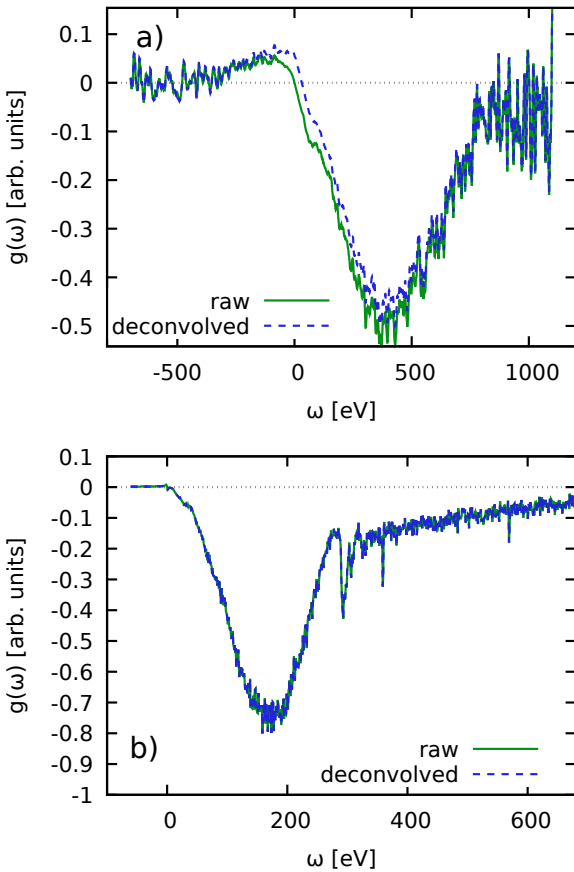


FIG. 1. Spectrally resolved contribution to the numerical derivative of the ITCF around $\tau = 0$, cf. Eqs. (1) and (2). Panels a) and b) correspond to the Be NIF shot (Fig. 2 of the main text) and the carbon XFEL shot (Fig. 3 of the main text), respectively, that are analyzed in the main text.

I. SPECTRALLY RESOLVED CONTRIBUTIONS TO THE NORMALIZATION

The spectrally resolved contribution to the numerical derivative defined by Eq. (6) in the main text is given by

$$g(\omega) = \lim_{\epsilon \rightarrow 0} f_\epsilon(\omega) , \quad (1)$$

with the definition

$$f_\epsilon(\omega) = \frac{I(\mathbf{q}, \omega)}{\epsilon} \left(\frac{e^{-\hbar\omega\epsilon}}{\mathcal{L}[R(\omega)](\epsilon)} - \frac{1}{\mathcal{L}[R(\omega)](0)} \right) . \quad (2)$$

Thus, Eq. (6) can be re-written as

$$A = -\frac{2m_e}{(\hbar q)^2} \int_{-\infty}^{\infty} d\omega g(\omega) . \quad (3)$$

In Fig. 1a), we show $g(\omega)$ for the Be NIF shot shown in Fig. 2 in the main text. Clearly, most contributions to the normalization come from positive scattering energies, $\omega > 0$. In fact, the absolute values of the contributions to A qualitatively follow $I(\mathbf{q}, \omega)$. This is in stark contrast to the ITCF thermometry method introduced in Refs. [1, 2], where negative frequencies contribute with a weight that exponentially increases with τ due to the exponent in the two-sided Laplace transform, cf. Eq. (2) of the main text. For completeness, we note that the slightly negative contributions around $\omega = 1$ keV are potentially spurious; a possible explanation for this artefact might be the employed background subtraction of the XRTS lineouts, which will be discussed in more detail in a dedicated future publication.

In Fig. 1b), we repeat this analysis for the carbon data shown in Fig. 3 of the main text. It can be seen that contributions for $\omega < 0$ are negligible in practice. In addition, we observe a fast, monotonic decrease of $g(\omega)$ with ω . The remaining contributions to the normalization beyond the available spectral range are, therefore, small, leading to the relatively small uncertainty in our final estimate for the normalized static static structure factor as $S_{ee}(\mathbf{q}) = 0.823 \pm 0.01$ for this example.

* t.dornheim@hzdr.de

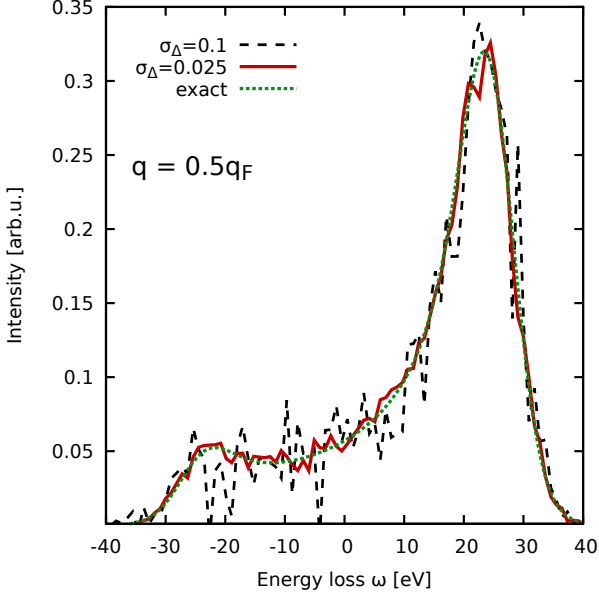


FIG. 2. Synthetic intensity computed for a pure UEG model [3, 4] with $r_s = 2$ and $\Theta = 1$ ($T = 12.53$ eV) for $q = 0.5q_F$. The dynamic structure factor has been convolved with a Gaussian instrument function of width $\sigma = 3.33$ eV. Dotted green: exact data; solid red and dashed black: perturbed with different noise levels σ_Δ , cf. Eq. (4).

II. STABILITY WITH RESPECT TO NOISE

An additional important question is the stability of the numerical derivative in Eq. (6) in the main text with respect to experimental noise. Following Refs. [2, 5], we express the experimental signal $I_{\text{exp}}(\mathbf{q}, \omega)$ as [2, 5]

$$I_{\text{exp}}(\mathbf{q}, \omega) = I(\mathbf{q}, \omega) + \xi_{\sigma_\Delta}(\omega) \sqrt{I(\mathbf{q}, \omega)}, \quad (4)$$

with $\xi_{\sigma_\Delta}(\omega)$ being a Gaussian random variable distributed around zero with σ_Δ being the variance. In Fig. 2, we show a synthetic intensity curve for a UEG model, see also Fig. 1 in the main text; the green curve shows the exact reference curve, and the solid red and dashed black lines have been perturbed with random noise with different values of σ_Δ .

To rigorously quantify the impact of the random noise onto the numerical derivative of the ITCF, we compute $K = 10^4$ noisy synthetic intensity signals for different values of σ_Δ . In Fig. 3, we show corresponding histograms (bars) for $\sigma_\Delta = 0.025$ (red) and $\sigma_\Delta = 0.1$ (blue). The solid green curves depict Gaussian fits that are in excellent agreement to the histograms. In other words, the presence of random noise governed by Eq. (4) leads to a Gaussian distribution of the slope of the corresponding ITCF around the exact value.

This can be seen particularly well in Fig. 4, where we show the mean value over $K = 10^4$ samples (green crosses) as a function of σ_Δ , with the error bars depicting the corresponding variance. Clearly, the mean values

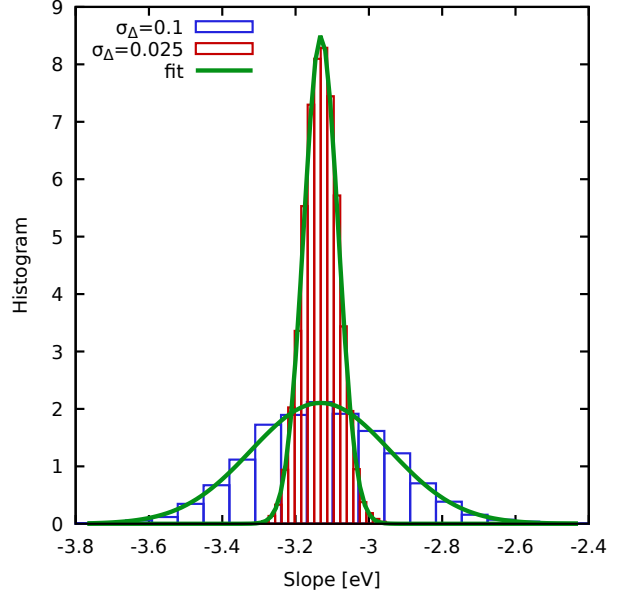


FIG. 3. Sampling $K = 10^4$ noisy intensity signals via Eq. (4) for each considered value of the noise level σ_Δ . Shown is the histogram of computed slopes from the K noisy I samples for $\sigma_\Delta = 0.1$ and $\sigma_\Delta = 0.025$, cf. Fig. 2.

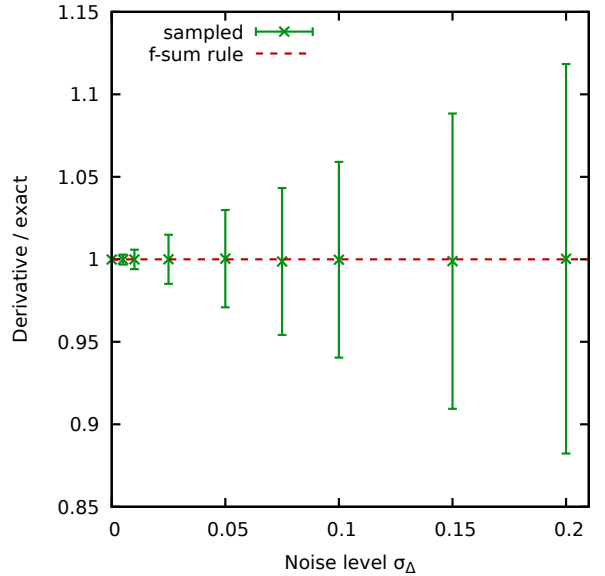


FIG. 4. Estimated variance of slope samples as a function of σ_Δ .

nicely reproduce the exact value (dashed red). Moreover, the variance appears to be linear with σ_Δ . Indeed, even for $\sigma_\Delta = 0.15$, corresponding to a noise level exceeding the fluctuations of the dashed black curve in Fig. 2, we find a variance within 10% of the exact normalization.

- [1] Tobias Dornheim, Maximilian Böhme, Dominik Kraus, Tilo Döppner, Thomas R. Preston, Zhandos A. Moldabekov, and Jan Vorberger, “Accurate temperature diagnostics for matter under extreme conditions,” *Nature Communications* **13**, 7911 (2022).
- [2] Tobias Dornheim, Maximilian P. Böhme, David A. Chapman, Dominik Kraus, Thomas R. Preston, Zhandos A. Moldabekov, Niclas Schlünzen, Attila Cangi, Tilo Döppner, and Jan Vorberger, “Imaginary-time correlation function thermometry: A new, high-accuracy and model-free temperature analysis technique for x-ray Thomson scattering data,” *Physics of Plasmas* **30**, 042707 (2023).
- [3] T. Dornheim, S. Groth, J. Vorberger, and M. Bonitz, “Ab initio path integral Monte Carlo results for the dynamic structure factor of correlated electrons: From the electron liquid to warm dense matter,” *Phys. Rev. Lett.* **121**, 255001 (2018).
- [4] Tobias Dornheim, Attila Cangi, Kushal Ramakrishna, Maximilian Böhme, Shigenori Tanaka, and Jan Vorberger, “Effective static approximation: A fast and reliable tool for warm-dense matter theory,” *Phys. Rev. Lett.* **125**, 235001 (2020).
- [5] J. Sheffield, D. Froula, S.H. Glenzer, and N.C. Luhmann, *Plasma Scattering of Electromagnetic Radiation: Theory and Measurement Techniques* (Elsevier Science, 2010).